Nonlinear IBVS Controller for the Flare Maneuver of Fixed-Wing Aircraft using Optical Flow

Pedro Serra, Florent Le Bras, Tarek Hamel, Carlos Silvestre and Rita Cunha

***Abstract*— This paper describes a nonlinear Image-Based Visual Servo controller for the Flare phase of the landing maneuver of a fixed-wing aircraft in presence of a wind gust. Optical-Flow and 2D image features of the runway are exploited to design a feedback controller for the automatic maneuver. The controller is divided in two components. The first guarantees the horizontal alignment with the center of the runway, using the two lines delimiting the runway represented through a modification of the so-called Plücker coordinates. The second component takes advantage of the Optical-Flow measurements to ensure a smooth touchdown. Finally simulation results are presented to illustrate the performance of the control approach.**

I. Introduction

Unmanned Aerial Vehicles (UAVs) have matured into a major research topic over the last decade. Significant effort has been placed on the development of both fixed-wing and rotary-wing aircrafts. As new sensor technology and increasingly powerful computational systems become available, their potential to perform high precision tasks in challenging and uncertain operation scenarios increases, demanding efficient motion control algorithms to perform all kinds of challenging maneuvers autonomously.

One major problem when designing control systems is the difficulty to accurately measure the vehicle's position regarding the local environment. GPS (Global Positioning System) is being widely used and is, nowadays, the primary navigation aid in most algorithms, see for example [3] and [17]. However, this approach presents some drawbacks: the GPS provides positioning information in the Earth-Centered, Earth-Fixed frame (ECEF) without considering local topography. The GPS measurement rate is not sufficient for some applications and the quality of the height's measure is poor. Also GPS signals are subjected to shortages in environments with many occlusions, for example, urban environments, and vulnerable to jamming effects. For these reasons there has been increasing interest in developing alternative systems to provide robust relative pose information that can be used instead of GPS in navigation algorithms. One alternative to GPS is the use of a vision system.

This work was partially supported by Fundação para a Ciência e a Tecnologia (ISR/IST plurianual funding) and by the project PTDC/EEAACR/72853/2006 HELICIM of the FCT and AIRTICI from AdI.

The work of P. Serra was supported by a PhD Student Grant from the FCT POCTI program, SFRH / BD / 36696 / 2007.

P. Serra, C. Silvestre and R. Cunha are with the Department of Electrical Engineering and Computer Science, and Institute for Systems and Robotics, Instituto Superior Técnico, 1049-001 Lisboa, Portugal. {pserra,cjs,rita}@isr.ist.utl.pt

F. Le Bras is with the Laboratoire de Recherches Balistiques et Aerodynamiques (LRBA) of the French Delegation Generale pour lArmement, Vernon, France, florent.le-bras@polytechnique.org

T. Hamel is with I3S UNSA-CNRS, Nice-Sophia Antipolis, France, thamel@i3s.unice.fr

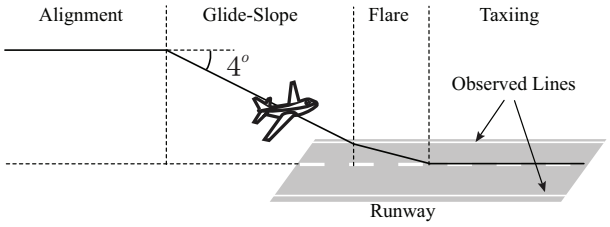

Fig. 1.

Using cameras as primary sensors for relative position allows to cast the problem into an Image-Based Visual Servo Control problem ([4], [5]), opening the possibility to perform autonomous tasks in low-structured environments with no external assistance, [6], [16], [10], [13], [7]. Aircraft landing is an example of such an application, where it would be interesting to develop control algorithms to perform the maneuver without assistance and ground equipment. The landing maneuver of an airplane is composed of four phases, see Figure 1:

- Alignment: in this phase the airplane has to align with the runway at a fixed desired altitude from the ground;
- Glide-slope: in this phase the airplane follows a straight-line descending path, while keeping the alignment with respect to the runway;
- Flare: when the airplane approaches the runway (about 20 meters for a Jet sized aircraft), a specific flare maneuver begins to lower the glide-path angle and ensure a touchdown with minimal vertical velocity;
- Taxiing: the last phase of the landing maneuver, begins when the airplane touches the runway. It acts as ground vehicle reducing its velocity.

This paper proposes a vision-based strategy to approach the problem of fixed-wing aircraft landing, addressing in particular the flare phase. This phase is the most critical and requires a well suited controller to ensure a smooth and damage-free touchdown.

The control architecture is decoupled into an inner-loop and outer-loop controller. The outer-loop controller stabilizes the translational (or guidance) dynamics resorting to visual data and using the sideslip angle and the angle of attack as control inputs. The inner-loop controller actuates on the aircraft control surfaces and provides high-gain stabilization of the vehicle's angle of attack, side-slip and roll angles based on direct measurements of the IMU and pitot tubes. The

Preprint submitted to 49th IEEE Conference on Decision and Control.
Received April 1, 2010.

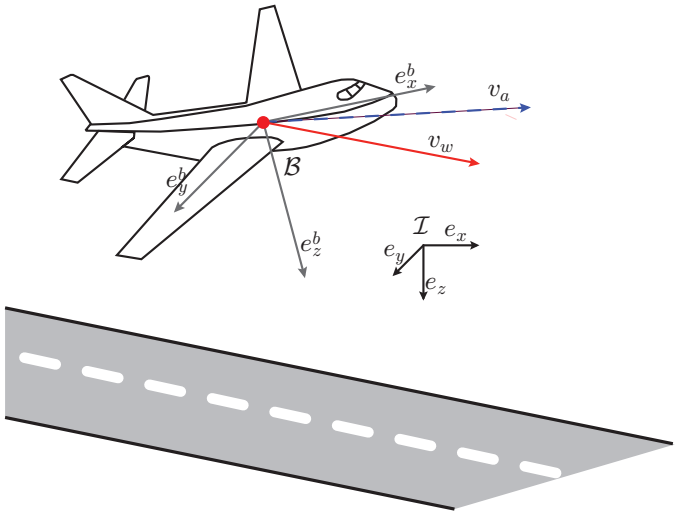

Fig. 2.

time-scale separation between the two loops is considered sufficient so that the interaction terms can be ignored in the control design. Detailed studies on the inner/outer loop approach of controllers design can be found in [11] and [2].

In [12] the authors present an IBVS controller for the Alignment and Glide-slope phases of the landing maneuver using the Plücker coordinates of the lines delimitating the runway. The proposed controller is divided in two components, the first uses new modified bi-normalized Plücker coordinates to maintain the airplane aligned with the center of the runway. The second component uses the vertical component of the optical-flow, also called optical-flow divergence, [8], and guarantees a smooth touchdown resorting to a specially suited Lyapunov function.

This paper is structured in four sections. Section II presents the dynamic model of an airplane. Section III presents the image features and derives a Lyapunov based controller for the considered problem. Section IV presents simulation results for the full nonlinear dynamics of an aircraft. The final sections provide a short summary of conclusions and future research directions.

II. Modeling

A. Aircraft dynamics

To describe the motion of the UAV, two reference frames are introduced: a fixed inertial frame $\mathcal{I}$ associated with the vector basis $[e_x, e_y, e_z]$ and a body-fixed frame, $\mathcal{B}$, attached to the vehicle's center of mass and associated with the vector basis $[e_x^b, e_y^b, e_z^b]$. The orientation of the aircraft is given by the rotation matrix $R \in \mathrm{SO}(3)$ from $\mathcal{B}$ to $\mathcal{I}$, which can be parameterized by the yaw, pitch and roll Euler's angles, denoted by ψ, θ and ϕ, respectively. The position of the vehicle's center of mass expressed in $\mathcal{I}$ is denoted by $\xi = (x, y, z)^T$ and the linear velocity, expressed in $\mathcal{B}$ is denoted by v and defined as the sum of the wind velocity v_w and the so-called airspeed v_a:

$$v = v_a + v_w. \tag{1}$$

The wind is assumed to be constant with respect to the inertial frame. Finally the angular velocity defined in $\mathcal{B}$ is denoted by $\Omega = (p, q, r)^T$. The kinematic and dynamic equations of motion for the vehicle can be written as

$$\dot{\xi} = Rv \tag{2}$$
$$m\dot{v} = -\mathrm{sk}(\Omega)mv + F \tag{3}$$
$$\dot{R} = R\mathrm{sk}(\Omega) \tag{4}$$
$$I\dot{\Omega} = -\mathrm{sk}(\Omega)I\Omega + \Gamma. \tag{5}$$

where m is the vehicle's mass, I is the moment of inertia and $\mathrm{sk}(.) : \mathbb{R}^3 \to \mathbb{R}^{3\times 3}$ denotes the matrix realization of the vectorial cross product: $\mathrm{sk}(\Omega)x = \Omega \times x$. The exogenous torque is denoted by Γ and the exogenous force is denoted by F and can be decomposed as

$$F = F_{\text{earth}} + F_{\text{engine}} + {}^{\mathcal{A}}_{\mathcal{B}}R^T F_{\text{aero}},$$

where $F_{\text{earth}} = mgR^T e_z^b$ is the gravitational force, $F_{\text{engine}} = Te_x^b$ where T is the thrust of engine turbines. F_{aero} is due to aerodynamical effects and is expressed in the aerodynamic airframe $\mathcal{A}$ as a function of the dynamic pressure $\bar{Q}$, angle of attack α, and sideslip angle β:

$$\frac{F_{\text{aero}}}{\bar{Q}S} = -C_X(\alpha,\beta)E_x^a + C_{Y,\beta}\beta E_y^a - C_{Z,\alpha}(\alpha - \alpha_0)E_z^a,$$

where $E_x^a = \frac{v_a}{\|v_a\|}$, $E_z^a = \frac{E_x^a \times e_y}{\|E_x^a \times e_y\|}$ and $E_y^a = E_z^a \times E_x^a$. The matrix ${}^{\mathcal{A}}_{\mathcal{B}}R \in \mathrm{SO}(3)$ is the rotation matrix from $\mathcal{B}$ to $\mathcal{A}$. The reference surface of the airplane is denoted by S, $(C_X, C_{Y,\beta}, C_{Z,\alpha})$ are the so-called aerodynamic coefficients and α_0 is the angle-of-attack that nullifies aircraft's lift.

The actuators for the dynamics (2)-(5) are the thrust of engine turbines T and orientation of control surfaces $(\delta_l, \delta_m, \delta_n)$ that allow to design the torque Γ as desired.

The approach used for the Flare phase of the landing maneuver consists in:

1) regulating the norm of the airspeed $V_a = \|v_a\|$ to a desired forward velocity V_a^d,
2) stabilizing the attitude dynamics (4)-(5) through a high gain inner loop controller such that assignments in (ϕ, α, β) are correctly performed,
3) stabilizing the translational dynamics (2)-(3) using (β, α) as guidance control inputs and considering $\phi = 0$ and V_a constant. This approach is particulary adapted for the flare maneuver because a landing system is used. For the other phases, the so-called bank-to-turn maneuver which consists in considering (α, ϕ) as guidance inputs along with the constraint $\beta = 0$, is classically used.

The first item requires the use of the propeller thrust to regulate the airspeed V_a towards the desired value V_a^d. Note that, in order to guarantee that the aircraft's dynamics (2)-(5) are controllable, the desired airspeed must be larger than the maximum between the wind amplitude $\|v_w\|$ and the lower speed threshold of the aircraft V_a^l:

$$V_a^d > \max\{\|v_w\|, V_a^l\}.$$

Preprint submitted to 49th IEEE Conference on Decision and Control.
Received April 1, 2010.

In practice, this limitation comes from the airplane design and characteristics. The airplane should not be used when the wind conditions are higher than a limit identified upon the airplane conception. Hence, the following assumption is done on wind velocity.

Assumption 1: There exists $\varepsilon \in [0, 1]$ such that:

$$\|v_w\| < \varepsilon V_a^d.$$

The second item is accomplished through a standard high-gain inner-loop whose description is omitted from this paper.

Finally to achieve the goal described in 3), the guidance dynamics, can be simplified by considering that the corresponding time constant is larger than those of the inner-loop controller and of the airspeed regulation. As such, it can be assumed that the airspeed is constant and the roll angle is null. Therefore the dynamics for the guidance control problem are described as

$$\begin{aligned}\dot{\xi} &= R(v_a + v_w)\\ \dot{v}_w &= -\mathrm{sk}(\Omega)v_w\\ \dot{v}_a &= -\mathrm{sk}(\Omega)v_a + \pi_{v_a}u_a(\alpha,\beta)\end{aligned}$$

where

$$\pi_{v_a} = I_d - \frac{v_a v_a^T}{V_a^2}$$

yields the projection on the plane orthogonal to v_a, and $u_a(\alpha, \beta)$ is the actuation provided by the guidance controller that can be described as

$$\begin{aligned}u_a(\alpha,\beta) \quad &= \left[\tfrac{\bar{Q}S}{m}C_{y,\beta}\beta - \mathrm{c}_\alpha\mathrm{s}_\beta\left(\tfrac{T}{m} - g\mathrm{s}_\theta\right) - g\mathrm{c}_\theta\mathrm{s}_\alpha\mathrm{s}_\beta\right]E_y^a +\\ &+ \left[g\mathrm{c}_\theta\mathrm{c}_\alpha - \tfrac{\bar{Q}S}{m}C_{z,\alpha}(\alpha-\alpha_0) - \mathrm{s}_\alpha\left(\tfrac{T}{m} - g\mathrm{s}_\theta\right)\right]E_z^a.\end{aligned} \tag{6}$$

The angle commands (α^c, β^c) to the inner-loop controller can be determined from (6), by solving a nonlinear system.

The proposed control strategy will depend only on the measurement of the following variables:

- the Euler angles (ϕ, θ, ψ) and angular velocity Ω, both provided by an Inertial Measurement Unit - IMU,
- the norm of the airspeed, angle of attack and sideslip angle $(|V_a|, \alpha, \beta)$, measured by pitot tubes and pressure intakes, and providing a direct measure of v_a
- and visual features extracted by a vision system.

The wind velocity cannot be measured but is estimated by the proposed control algorithm. The aircraft position is unknown, however the visual features used provide sufficient information to align the aircraft with the runway and perform the maneuver without complementary position measurements.

III. Choice of Image features

In this section image features are derived. It is assumed that the target is the runway on a textured ground. The borders of the runway will be used the perform the alignment of the aircraft while textures are exploited to perform the vertical landing.

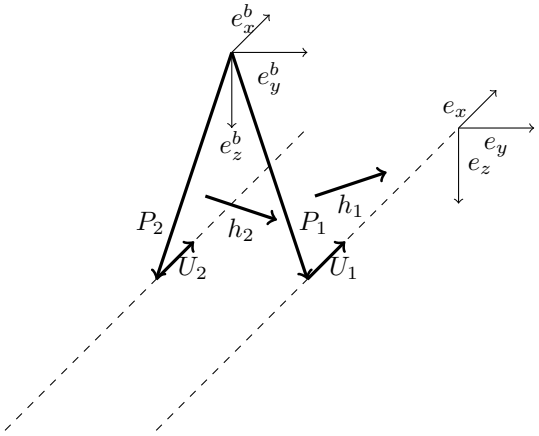

Fig. 3. Sketch of airplane position

A. Modified Plücker coordinates

Consider a collection of $n \geq 2$ parallel lines. Let $u \in \mathcal{I}$ and $U \in \mathcal{B}$ ($U = R^T u$) denote the unit direction of the lines. The camera-fixed frame is assumed to coincide with $\mathcal{B}$ and the image features are assumed to remain in the camera's field of view during flight.

Based on the images of the parallel lines, we are interested in defining a visual feature that encodes the alignment error with respect to the runway. More specifically, the visual feature should be such that zero error is achieved only when the aircraft's position lies on a plane orthogonal to the center of the runway.

The visual features are represented through a modification of the so-called bi-normalized Plücker coordinates. Plücker coordinates are an explicit representation of straight lines in 3-D space, which simplify technically the development of the proposed control approach, [16], [12]. Using these coordinates, a line is represented by the unit vector $h_i \in \mathcal{B}$ orthogonal to the plane containing both the line and the origin of the reference frame $\mathcal{B}$. Note that $h_i \in \mathcal{B}$ can be written as

$$h_i = \frac{H_i}{\|H_i\|} = \frac{P_i \times U}{\|P_i \times U\|}$$

where $H_i = P_i \times U$ and P_i denotes the vector between the camera and an arbitrary point on the image of the *i*-th parallel line, see Figure 4. The images provide direct measurements of h_i and U can be obtained from $U = \frac{h_i \times h_j}{\|h_i \times h_j\|}$, for $i \neq j$.

In previous work, measurements h_i were directly used to design a centroid vector $q := \sum h_i$ which encoded the 2D pose information needed for stabilization on the trajectory parallel to the runway [12]. The IBVS task consisted therefore in stabilizing q on a desired centroid vector q^*. In this new approach, a new vector is designed to stabilize only the horizontal movement, while an optical-flow based controller will stabilize the vertical motion.

The positioning error is dealt through the so-called centroid vector q. The centroid information is commonly used in visual servo control [1], [6] and can be defined as the sum of

the Plücker coordinates. However we propose a modification to the Plücker coordinates that requires the definition of a desired centroid vector $q^* := R^T b^*$, where b^* is a constant vector that encodes the desired position information. For this case we consider $b^* = e_y$. Thus let the new modified Plücker coordinates be defined as

$$g_i = \pi_{q^*} h_i$$

where $\pi_{q^*} = I_d - \frac{q^* q^{*T}}{\|q^*\|^2}$. Note that g_i is the projection of h_i in the orthogonal plane to q^*. Thus, the centroid vector can be defined as

$$q := \sum g_i = \pi_{q^*} \sum g_i.$$

Note that when $q = 0$ the airplane must be at center of the lines, i.e. the sum of the h_i vectors is in the direction of q^*, see Figure 4.

The time derivative of H_i is given by [16]

$$\dot{H}_i = -\mathrm{sk}(\Omega) H_i - v \times U,$$

Thus the dynamics of g_i can be described as

$$\dot{g}_i = -\mathrm{sk}(\Omega) g_i - \frac{1}{\|H_i\|} \pi_{q^*} \pi_{h_i} (v \times U).$$

Finally the time derivative of the centroid vector is given by

$$\dot{q} = -\mathrm{sk}(\Omega) q - \pi_{q^*} Q (v \times U) \tag{7}$$

where

$$Q = \sum \frac{1}{\|H_i\|} \pi_{h_i}. \tag{8}$$

Q is a positive definite matrix as long as there are at least two ($n \geq 2$) visible features [16]. This property is exploited in the control design and avoids the need to estimate it. Nevertheless, some bounds are required on the trajectories considered, to avoid ill-conditioning of the eigenvalues of Q. In this development, we define a region of space by a pair of uniform bounds on the matrix

Assumption 2: There exist two positive scalars $(q_m, q_x) > 0$ such that:

$$q_m < \{\lambda_i(Q)\} < q_x.$$

This is a classical assumption for IBVS control schemes. Recalling (8), q_m limits the distance between the airplane and the runway, while q_x, the upper-bound, implies that the ground is not touched by the camera.

B. Translational Optical Flow

Consider the dynamics of an image point, also called optical-flow, under spherical projection of a camera with unit image radius, [15], [9], [14]:

$$\dot{p} = -\mathrm{sk}(\Omega) p - \frac{\cos\theta_p}{d(t)} \pi_p v \tag{9}$$

where $d := d(t)$ is the orthogonal distance from the target surface to the origin of frame $\mathcal{B}$ measured as a positive scalar, and θ_p is the angle between the inertial direction η and the observed target point p.

The visual velocity measure that is used is the translational optical flow w, expressed in the inertial frame:

$$w(t) = \frac{V}{d} = \frac{Rv}{d}.$$

When the observed world is a flat planar surface, translational optical flow will have three components, flow in the two planar directions, analogous to classical optical flow, and flow in the normal direction to the plane, analogous to optical divergence.

Measuring the translational optical flow is a key aspect of the practical implementation of control algorithms proposed.

The optical flow $\dot{p}$ can be computed using a range of algorithms (correlation-based technique, features-based approaches, differential techniques, etc) [18]. Note that due to the rotational ego-motion of the camera, (9) involves the angular velocity as well as the linear velocity [17].

An effective measurement of w is obtained by integrating the observed optical flow over a section $\mathcal{W}^2$ of the sphere around the pole normal to the target plane, [15]:

$$\phi = \int\int_{\mathcal{W}^2} \dot{p} = -\beta_f \Omega \times \eta - \frac{Q_f v}{d}, \tag{10}$$

where β_f represents the angle of the field of view of the window $\mathcal{W}^2$ and $Q_f = R^T (R_t \Lambda R_t^T) R$ is a symmetric positive definite matrix. The matrix Λ is a constant diagonal matrix depending on the window parameters and R_t represents the rotational matrix from the target plane to the inertial frame.

From (10) is straightforward to obtain the translational optical flow:

$$w = (w_x, w_y, w_z)^T = -(R_t \Lambda^{-1} R_t^T) R (\phi + \mu \Omega \times \eta)$$

Note that if the target frame coincides with the inertial plane, $R_t = I_d$, then the normal direction to the target becomes e_z (observed from the camera-frame as vector pointing towards the plane). Moreover, if one assumes that if the target plane is in the plane $x - y$ of the inertial frame, the variable d becomes the height h (or $|z|$) from the camera to the target.

IV. Problem formulation

Let w^* be the constant desired translational optical flow divergence. It is straightforward to show that when $w_z = w^*$ one has $\dot{h} = -h_0 w^* \exp(-w^* t)$ and $h = h_0 \exp(-w^* t)$ which converges to zero and ensuring a smooth landing.

The IBVS stabilization task consists in driving exponentially the centroid vector q to the desired one, q^* (i.e. $q - q^* \to 0$) in the direction orthogonal to q^* resulting in the alignment of the airplane in the center of the runway, and also regulate $\frac{\dot{h}}{h} + w^*$. Thus, two error terms are introduced:

$$\begin{aligned} \delta =& \pi_{q^*} q \\ \delta_3 =& q_0^* \dot{h} = q_0^* q_0^{*T} \mathrm{sk}(U) v \end{aligned} \tag{11}$$

where $q_0^* = \frac{q^*}{|q^*|}$ and $\dot{h} = q_0^{*T} (v \times U)$ is the time derivative of the height of the aircraft's center of mass. Hence the control approach is divided in two parts. In the first part, δ is driven to zero ensuring the horizontal alignment and in the second part a control law is chosen to guarantee the touchdown.

Preprint submitted to 49th IEEE Conference on Decision and Control.
Received April 1, 2010.

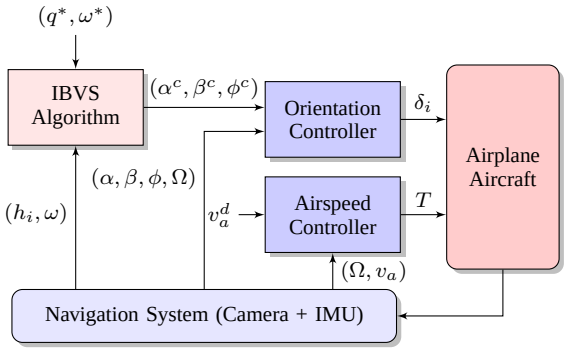

Fig. 4. Implementation block diagram.

A. Horizontal alignment

Combining the dynamics of equation (7) and an estimation of the wind velocity, the dynamics of the error term δ can be described as

$$\begin{aligned}\dot{\delta} =& -\mathrm{sk}(\Omega)\delta + \pi_{q^*} Q \pi_{q^*} \mathrm{sk}(U) v + \pi_{q^*} Q \delta_3 \\ =& -\mathrm{sk}(\Omega)\delta + \pi_{q^*} Q \pi_{q^*} [\mathrm{sk}(U) v_a - \hat{v}_w - \tilde{v}_w] + \bar{\delta}_3\end{aligned} \tag{12}$$

where $\tilde{v}_w = v_w \times U - \hat{v}_w$ and $\hat{v}_w$ is an estimate of $v_w \times U$.

Choose the following dynamics for $\hat{v}_w$:

$$\dot{\hat{v}}_w = -\mathrm{sk}(\Omega)\hat{v}_w + \mathbf{P}\pi_U u_w, \qquad \hat{v}_w(0) = 0 \tag{13}$$

where u_w acts as the input of the wind estimator and

$$\mathbf{P} = \varepsilon' V_a \sqrt{1 - \frac{\|\hat{v}_w\|^2}{\varepsilon'^2 V_a^2}} \left(I - \frac{\hat{v}_w \hat{v_w}^T}{\varepsilon'^2 V_a^2} \right), \quad \varepsilon' \in \left(\frac{1+\varepsilon}{2}, 1 \right). \tag{14}$$

This wind velocity estimation remains in the plan orthogonal to U and ensures the norm of the wind estimate $\|v_w\|$ is strictly lower than $\varepsilon' V_a$. More details on this estimator can be found in [12].

Consider the following storage function, where k_1 is a positive control gain:

$$S_1 = \|\delta\|^2 + \frac{2}{k_1}(\pi_{q^*}\tilde{v}_w)^T \delta + \frac{4}{k_1^2}\|\pi_{q^*}\tilde{v}_w\|^2$$

choosing u_w as follows:

$$u_w = -k_2 \delta, \qquad k_2 > 0 \tag{15}$$

let v_a^d be the virtual commanded airspeed defined as

$$v_a^d := \mathrm{sk}(U)(k_1\delta - \hat{v}_w) + \sqrt{V_a^2 - \|k_1\delta - \hat{v}_w\|^2} U. \tag{16}$$

It can be verified that $\|v_a^d\| = V_a$. Knowing that $\delta < 2n$ and $\|\hat{v}_w\| < \varepsilon' V_a$, and choosing k_1 such that

$$k_1 < \frac{1-\varepsilon'}{2n} V_a \tag{17}$$

it can be ensured that v_a^d is correctly defined since

$$\|k_1\delta - \hat{v}_w\| < V_a$$

Introducing a new error term defined as:

$$\delta_2 = \pi_{q^*}\mathrm{sk}(U)(v_a - v_a^d)$$

and recalling (12), (13), (15) and (16), the derivative of the storage function can be described as

$$\begin{aligned}\dot{S}_1 =& 2\left(\delta + \frac{\pi_{q^*}\tilde{v}_w}{k_1}\right)^T Q\delta_2 + \\ &+ \frac{2k_2}{k_1}\left(\delta + \frac{4}{k_1}(\pi_{q^*}\tilde{v}_w)\right)^T \mathbf{P}\delta \\ &- 2k_1\left(\delta + \frac{\pi_{q^*}\tilde{v}_w}{k_1}\right)^T Q\left(\delta + \frac{\pi_{q^*}\tilde{v}_w}{k_1}\right) + \\ &+ 2\left(\delta + \frac{\pi_{q^*}\tilde{v}_w}{k_1}\right)^T \bar{\delta}_3\end{aligned}$$

Consider now a second storage function

$$S_2 = \frac{1}{2}\|\delta_2\|^2,$$

along with the dynamics of δ_2

$$\begin{aligned}\dot{\delta}_2 =& -\mathrm{sk}(\Omega)\delta_2 + \pi_{q^*}\mathrm{sk}(U)\pi_{v_a} u_a + k_1 \pi_{q^*} Q \delta_2 + \\ &- k_1^2 \pi_{q^*} Q\left(\delta + \frac{\pi_{q^*}\tilde{v}_w}{k_1}\right) - k_2 \pi_{q^*} P \delta + k_1 \bar{\delta}_3\end{aligned} \tag{18}$$

one can verify that the time derivative of the second storage function is given by:

$$\begin{aligned}\dot{S}_2 =& \delta_2^T \pi_{q^*}\mathrm{sk}(U)\pi_{v_a} u_a + k_1 \delta_2^T Q \delta_2 + \\ &- k_1^2 \delta_2^T Q\left(\delta + \frac{\pi_{q^*}\tilde{v}_w}{k_1}\right) - k_2 \delta_2^T \mathbf{P}\delta + \\ &+ k_1 \delta_2^T \bar{\delta}_3.\end{aligned} \tag{19}$$

The following proposition presents the controller that guarantees the horizontal alignment.

Theorem 1: Consider the dynamics defined by (12) and (18) along with (16). Assume that v_a^d is not in the opposite direction of v_a, i.e.

$$\exists \varepsilon_a > 0 \quad | \quad 1 - \cos(v_a, v_a^d) < 2 - \varepsilon_a.$$

and $\|\bar{\delta}_3\|$ is bounded by Ae^{-bt} with positive scalars A and b. Then choosing the control

$$\pi_{q^*}\mathrm{sk}(U)\pi_{v_a} u_a = -k_3 \delta_2 \tag{20}$$

positive gains (k_1, k_2, k_3, K) exist, such that the function

$$\mathcal{L} = S_1 + K S_2$$

is a Lyapunov function for the guidance dynamics that guarantees that the closed-loop solution exists for all time and the error signals $(\delta, \delta_2, \tilde{v}_w)$ converge to zero.

Proof: Consider the first term of (19) and introduce the control (20). Given that $\|v_a^d\| = V_a$, it can be written as:

$$\delta_2^T \pi_{q^*}\mathrm{sk}(U)\pi_{v_a} u_a = -k_3 \|\delta_2\|^2$$

Then using Schwarz inequality $X^T Y \leq \frac{1}{2}(|x|^2 + |y|^2)$, and noticing that

$$\|\delta\| \leq \sqrt{\mathcal{L}}$$

$$\|\pi_{q^*}\tilde{v}_w\| \leq \frac{k_1}{2}\sqrt{\mathcal{L}}$$

$$\|\delta_2\| \leq \sqrt{2K\mathcal{L}}$$

the derivative of $\mathcal{L}$ can be written as:

$$\dot{\mathcal{L}} \leq f_1 + f_2 \tag{21}$$

where

$$f_1 \leq -k_3 K \|\delta_2\|^2 + K\delta_2^T \left[\left(\frac{1}{K} + \frac{k_1^2}{2} + k_1 \right) Q - \frac{k_2}{2}\mathbf{P} \right] \delta_2$$

$$+ y^T \left[\left(-2k_1 + 1 + \frac{k_1^2 K}{2} \right) Q + \frac{4k_2}{k_1}\mathbf{P} \right] y +$$
$$- k_2 \left(\frac{K}{2} + \frac{2}{k_1} \right) \delta^T \mathbf{P} \delta$$

with $y = \left(\delta + \frac{\pi_{q^*}\tilde{v}_w}{k_1} \right)$ and

$$f_2 = (2y + \delta_2)^T \bar{\delta}_3 \leq c_1 \sqrt{\mathcal{L}} A \tag{22}$$

Recalling assumption 2, and noticing that one can ensure that f_1 is upper-bounded by a definite negative expression of $(\mathbf{P}\delta, \delta + \frac{\pi_{q^*}\tilde{v}_w}{k_1}, \delta_2)$ as soon as the control gains satisfy:

$$K < \frac{4k_1 - 2}{k_1^2} \tag{23}$$

$$k_2 < \frac{k_1 q_m}{4\varepsilon' V_a} \left(2k_1 - 1 - \frac{k_1^2 K}{2} \right) \tag{24}$$

$$k_3 > \left(\frac{1}{K} + \frac{k_1^2}{2} + k_1 \right) q_x + \frac{k_2}{2}\varepsilon' V_a. \tag{25}$$

Therefore $f_1 \leq -c_2\mathcal{L}$ where $c_2 > 0$ is a function of the gains $(k_1, k_2, k3, K)$. Using this property along with (22), equation (21) yields to

$$\dot{\mathcal{L}} \leq -c_2\mathcal{L} + c_1\sqrt{\mathcal{L}}A$$

Let $m = \sqrt{\mathcal{L}}$, then

$$\dot{m} = \frac{\dot{\mathcal{L}}}{\sqrt{\mathcal{L}}} < -c_2 m + c_1 A.$$

Hence, if there exists c_2 that satisfies

$$c_2 > \frac{c_1 A}{m(0)} \tag{26}$$

then m decreases for all time which implies that $\mathcal{L}$ also decreases for all time. Given the conditions for the gains in expressions (17) and (23)-(25), one can verify that it is possible to choose K, k_1 and k_2 small enough and k_3 large enough so that (26) is satisfied.

Thus Lyapunov direct method ensures that $(\mathbf{P}\delta, \delta + \frac{\pi_{q^*}\tilde{v}_w}{k_1}, \delta_2)$ converge to zero. Given the definition of $\mathbf{P}$, we note that it is positive definite as soon as $\hat{v}_w < \varepsilon' V_a$. Recalling (17) and the definition of ε' given in (14), and note that $\delta + \frac{\pi_{q^*}\tilde{v}_w}{k_1} = 0$ implies that

$$\|\hat{v}_w\| \leq 2nk_1 < (1 - \varepsilon')V_a < \varepsilon' V_a$$

Thus, being $\mathbf{P}$ a definite positive matrix at the equilibrium, it implies that $(\delta, \pi_{q^*}\tilde{v}_w, \delta_2)$ converge towards zero exponentially. ■

Remark 1: The proof is based upon the assumption that δ_3 is exponentially convergent. This is proved to be true in the next section.

Remark 2: Note that although the proposed controller guarantees exponential stability for the estimation error $\tilde{v}_w$, the initial condition of the estimator should not be arbitrary due to the intrinsic risk of the Flare maneuver, any kind of transient responses must be avoided. Thus, the initial condition of the estimator is inherited from the glide-slope controller, which has already a steady estimative for the wind velocity.

B. Touchdown control

The time derivative of (11) is given by

$$\dot{\delta}_3 = q_0^* q_0^{*T} \mathrm{sk}(U) \pi_{v_a} u_a(\alpha, \phi) \tag{27}$$

Theorem 2: Consider the dynamics of equation (27) with the control input defined as

$$q_0^* q_0^{*T} \mathrm{sk}(U) \pi_{v_a} u_a = -k_4 q_0^* \left(\frac{\dot{h}}{h} + w^* \right) \tag{28}$$

then the closed-loop system is Globally Exponentially Stable and therefore δ_3 converges exponentially to zero.

Proof: Assume that $\dot{h}$ is bounded and let χ be a Lyapunov function candidate defined by

$$\chi = h \exp\left\{ \frac{\dot{h}}{k_4} \right\}$$

It's time derivative is given by

$$\dot{\chi} = -w^* h \exp\left\{ \frac{\dot{h}}{k_4} \right\} = -w^* \chi$$

This ensures that χ converges exponentially to zero. It is straightforward to verify that if $\dot{h}$ is bounded, then h converges exponentially to zero. Consequently, it remains to show that $\dot{h}$ is bounded. Knowing that $h(0) > 0 \Rightarrow h(t) > 0$, let V be a second Lyapunov function candidate:

$$V = \frac{1}{2}\dot{h}^2 + k_1 w^* h$$

with time derivative given by

$$\dot{V} = -k_4 \frac{\dot{h}^2}{h}$$

Hence $V(t) < V(0)$ and then $|\dot{h}| < \beta, \forall_{t>0}$. Therefore h converges exponentially to zero and $\dot{h}$ also converges exponentially to zero. Consequentially δ_3 converges exponentially to zero. ■

C. Total Control law

Equations (20) and (28) can be added resulting in the following control law

$$\pi_U u_\alpha = \mathrm{sk}(U) k_3 \delta_2 + \mathrm{sk}(U) k_4 q_0^* \left(\frac{\dot{h}}{h} + w^* \right) \tag{29}$$

where

$$u_\alpha = \pi_{v_a} u_a = u_1 E_y^a + u_2 E_z^a.$$

Preprint submitted to 49th IEEE Conference on Decision and Control.
Received April 1, 2010.

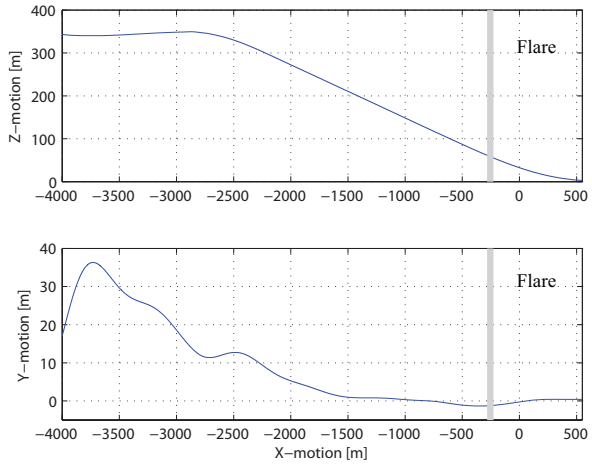

Fig. 5. Airplane position.

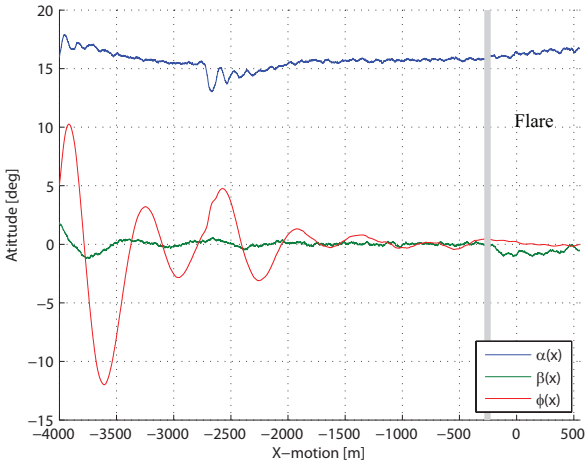

Fig. 6. Airplane attitude (ϕ, α, β).

Then choosing

$$u_1 = E_y^{aT}\left[\mathrm{sk}(U)k_3\delta_2 + \mathrm{sk}(U)k_4 q_0^*\left(\frac{\dot{h}}{h} + w^*\right)\right]$$

$$u_2 = \frac{E_z^{U^T}}{E_z^{U^T}E_z^a}\left[\mathrm{sk}(U)k_3\delta_2 + \mathrm{sk}(U)k_4 q_0^*\left(\frac{\dot{h}}{h} + w^*\right)\right]$$

with $E_z^U = e_y \times U$, ensures that the desired control equations (29) and (6) are verified.

V. Simulation Results

In this section, full dynamics of the jet-sized aircraft described in section II, are simulated and the visual guidance control law is tested in presence of wind. The aircraft model incorporates the nonlinear flight dynamics including aerodynamic effects and saturation on control surfaces deflection and thrust. Simulations have been undertaken with a specific simulation architecture of the LRBA, termed A^3.

The results presented include the full landing mission, alignment, glide-slope and flare phases, although this paper is focused only on the flare. Details about the controller used for the alignment and glide-slope can be found in [12]. The runway is aligned with the e_x axis and is 60 meters width. The desired trajectory consists in an alignment in the runway axis, 350m above the ground level, followed by a $4°$ glide-path maneuver starting when the aircraft is 4000m far from the runway. Finally the flare maneuver starts to ensure a smooth touchdown. The initial position is about 60m along the lateral direction, 25m along the vertical axis, and 7000m from the beginning of the runway (longitudinal position). For this simulation, the desired aerial velocity is:

$$V_a = 80ms^{-1}$$

Figures 5 and 6 show the aircraft position and attitude (ϕ, α, β) along the forward motion. Figure 6 present the attitude only for the flare phase. The results were obtained submitting the aircraft to lateral wind of $10m/s$.

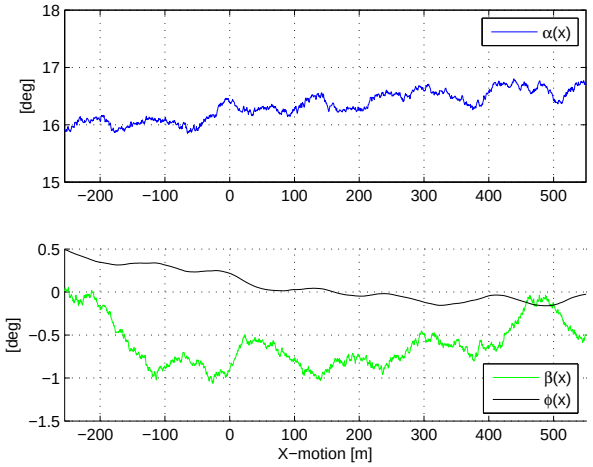

Fig. 7. Airplane attitude (ϕ, α, β) - Flare phase.

VI. Concluding remarks

This paper proposed a robust nonlinear IBVS controller for fixed-wing aircraft, without direct measurement of the aircraft position. The proposed controller allows the airplane to perform the Flare phase of the landing maneuver autonomously through a feedback on visual features. The controller performs the stabilization task along with bounded estimation of the wind. The control algorithm has been theoretically proved and tested in simulation with a nonlinear aircraft model. Results show that the control approach is suitable for the task and is robust to wind gust. Future work includes image treatment in the simulation architecture along with pan & tilt camera to ensure that the target surface is always visible.

References

[1] Russell L. Anderson. *A robot ping-pong player: experiment in real-time intelligent control*. MIT Press, Cambridge, MA, USA, 1988.

Preprint submitted to 49th IEEE Conference on Decision and Control.
Received April 1, 2010.

[2] S. Bertrand, T. Hamel, and H. Piet-Lahanier. Trajectory tracking of an unmanned aerial vehicle model using partial state feedback. In *European Control Conference*, 2007.

[3] D. Cabecinhas, C. Silvestre, P. Rosa, and R. Cunha. Path following control for coordinated turn aircraft maneuvers. In *AIAA Guidance and Control Conference*, 2007.

[4] F. Chaumette and S. Hutchinson. Visual servo control, part i: Basic approaches. *IEEE Robotics and Automation Magazine*, 13(4):82–90, December 2006.

[5] F. Chaumette and S. Hutchinson. Visual servo control, part ii: Advanced approaches. *IEEE Robotics and Automation Magazine*, 14(1):109–118, March 2007.

[6] N. Guenard, T. Hamel, and R. Mahony. A practical visual servo control for an unmanned aerial vehicle. *Robotics, IEEE Transactions on*, 24(2):331 –340, april 2008.

[7] T. Hamel and R. Mahony. Visual servoing of an under-actuated dynamic rigid-body system: an image-based approach. *Robotics and Automation, IEEE Transactions on*, 18(2):187–198, Apr 2002.

[8] B. Herisse, F.-X. Russotto, T. Hamel, and R. Mahony. Hovering flight and vertical landing control of a vtol unmanned aerial vehicle using optical flow. In *Intelligent Robots and Systems, 2008. IROS 2008. IEEE/RSJ International Conference on*, pages 801–806, Sept. 2008.

[9] Bruno Herisse, Tarek Hamel, Robert Mahony, and Francois-Xavier Russotto. A nonlinear terrain-following controller for a vtol unmanned aerial vehicle using translational optical flow. In *Robotics and Automation, 2009. ICRA '09. IEEE International Conference on*, pages 3251–3257, May 2009.

[10] Minh-Duc Hua, T. Hamel, P. Morin, and C. Samson. A control approach for thrust-propelled underactuated vehicles and its application to vtol drones. *Automatic Control, IEEE Transactions on*, 54(8):1837–1853, Aug. 2009.

[11] Alberto Isidori, Lorenzo Marconi, and Andrea Serrani. *Robust Autonomous Guidance*. Springer-Verlag New York, Inc., Secaucus, NJ, USA, 2003.

[12] F. Le Bras, T. Hamel, C. Barat, and R. Mahony. Nonlinear image-based visual servo controller for automatic landing guidance of a fixed-wing aircraft. In *European Control Conference*, pages 1836–1841, Aug. 2009.

[13] F. Le Bras, T. Hamel, and R. Mahony. Visual servoing of a vtol vehicle using virtual states. In *Decision and Control, 2007 46th IEEE Conference on*, pages 6442–6447, Dec. 2007.

[14] F. Le Bras, T. Hamel, and R. Mahony. Image-based visual servo control for circular trajectories for a fixed-wind airfcraft. In *Decision and Control, 2009 and 28th Chinese Control Conference. CDC-CCC '09. 48th IEEE Conference on*, Dec. 2009.

[15] R. Mahony, P. Corke, and T. Hamel. Dynamic image-based visual servo control using centroid and optic flow features. *Journal of Dynamic Systems, Measurement, and Control*, 130(1):011005, 2008.

[16] R. Mahony and T. Hamel. Image-based visual servo control of aerial robotic systems using linear image features. *Robotics, IEEE Transactions on*, 21(2):227–239, April 2005.

[17] P. Rosa, C. Silvestre, D. Cabecinhas, and R. Cunha. Autolanding controller for a fixed wing unmanned air vehicle. In *AIAA Guidance and Control Conference*, 2007.